Polarimetric Radar Observations of Biological Scatterers in Hurricanes Irene (2011) and Sandy (2012)

MATTHEW S. VAN DEN BROEKE

Department of Earth and Atmospheric Sciences, University of Nebraska–Lincoln, Lincoln, Nebraska

(Manuscript received 25 February 2013, in final form 31 July 2013)

ABSTRACT

Biological scatterers, consisting of birds and insects, may become trapped near the circulation center of tropical cyclones, particularly if a well-developed eyewall is present. These scatterers may be observed using weather radar, where they may appear to the radar operator as areas of light precipitation. Polarimetric radar characteristics of these scatterers, informed by additional observations of known bioscatter, include a combination of very high differential reflectivity (3–7.9 dB) and very low copolar correlation coefficient (0.3–0.8). Polarimetric radar observations of bioscatter are presented for Hurricane Irene (2011) and Hurricane Sandy (2012). In these storms, the bioscatter signature first appeared at the 0.5° elevation angle at a distance of 100–120 km from the radar. The signature appeared on successively higher tilts as the circulation center neared the radar, and its areal coverage in constant altitude plan position indicator (CAPPI) slices was primarily governed by the distribution of convection in the eye and by the timing of landfall. The highest altitude at which the signature appears may represent the inversion level within certain tropical cyclone eyes. For Hurricane Irene, inland observations of oceanic bird species support biological transport. Knowledge of the bioscatter signature has value to meteorologists monitoring tropical cyclones within the range of a polarimetric radar, possible value for estimating inversion height changes within the eyes of well-structured tropical cyclones, and value to biologists who wish to estimate the magnitude of biological transport in tropical cyclones.

1. Introduction and motivation

Scatterers detected by weather radar may be meteorological (e.g., raindrops, hailstones) or nonmeteorological in nature (e.g., aircraft, tornado debris; Ryzhkov et al. 2005). Biological scatterers (e.g., insects, birds, bats) constitute a special case of nonmeteorological targets, and represent an ubiquitous source of weather radar signal return, particularly during migration and throughout the warm season (e.g., Gauthreaux and Belser 1998). Single-polarization radars have poor ability to distinguish biological scatterers (bioscatter) from meteorological targets, and such distinction has required the data interpreter to know something of local ecology (e.g., O'Neal et al. 2010). With the advent of widespread polarization diversity, including the ongoing upgrade of the Weather Surveillance Radar-1988 Doppler (WSR-88D) network, it is now often possible to differentiate bioscatter from other meteorological and nonmeteorological sources of radar echo. For the first time, a widespread tool will be available that allows remote sensing of bioscatter movement (e.g., migration; roost dispersal) and transport (e.g., birds and insects carried in the eye of a tropical cyclone).

Polarization diversity yields an additional set of variables that can be used to infer dominant scatterer shape and phase (Bringi and Chandrasekar 2001). Polarimetric radar variables included in the upgraded WSR-88D network are reflectivity factor (Z_{HH}), differential reflectivity (Z_{DR}), copolar correlation coefficient (ρ_{hv}), and specific differential phase (K_{DP}). With knowledge of typical values of these variables for particular scatterer types, one may aggregate probabilities for each scatterer classification from each polarimetric variable in a given sample volume, and thus determine the most likely scatterer type in that volume. This approach is called fuzzy logic (Straka et al. 2000; Park et al. 2009).

A few studies have presented radar observations of bioscatter. Prior to the widespread availability of polarimetric observations, birds were frequently observed. Movement and roosting behavior of purple martins

Corresponding author address: Matthew S. Van Den Broeke, Department of Earth and Atmospheric Sciences, University of Nebraska–Lincoln, 306 Bessey Hall, Lincoln, NE 68588-0340.
E-mail: mvandenbroeke2@unl.edu

DOI: 10.1175/JTECH-D-13-00056.1

© 2013 American Meteorological Society

(*Progne subis*) has been studied (Russell et al. 1998) on the basis of a characteristic expanding annulus of Z_{HH} that accompanies morning roost dispersal. Bird density during migration has been estimated near the Great Lakes (Diehl et al. 2003), assuming a typical cross section for a migratory land bird and directly relating radar reflectivity to total scatterer cross section in a radar sample volume. Methods using Z_{HH}, radial velocity, and the velocity–azimuth display (VAD) to classify bioscatter have been used to identify best conservation practices by determining preferred habitats utilized by birds during migration (Bonter et al. 2009). In a recent migration study, radar echoes were confirmed via thermal infrared imaging to correspond to scatterers with the same cross section as dabbling ducks (O'Neal et al. 2010)—these echoes corresponded to known local migratory movements, and ground estimates of duck concentration correlated well with radar reflectivity ($R^2 = 0.91$). An algorithm has been developed to identify bioscatter in nonpolarimetric radar data during nighttime Great Plains migration events (Lakshmanan et al. 2010), where properties of bioscatter may be quite similar to those of stratiform precipitation.

Bats and insects have also been studied using nonpolarimetric radar data. Bats often emerge from caves in large numbers around sunset, particularly Mexican free-tailed bats (*Tadarida brasiliensis*) in Texas and Oklahoma. Evening dispersion patterns have been studied for these bats (Horn and Kunz 2008; Frick et al. 2012), and it may be possible to derive number density of bats or other bioscatterers using radar data (Chilson et al. 2012a). Insect scattering properties using nonpolarimetric radar have also been occasionally examined. A review of these studies, and the multitude of radar applications to insect behavior, is given by Chapman et al. (2011). Radar applications to bioscatter are summarized by Gauthreaux and Belser (1998) and Chilson et al. (2012b).

Polarimetric radar studies of bioscatter are relatively scarce. Insect concentrations attributed to grasshoppers have been identified along gust fronts as regions where Z_{DR} reaches 8–9 dB (Achtemeier 1991). Absolute Z_{DR} values may vary depending on scatterer orientation and size. Insect-dominated bioscatter has also been associated with high Z_{DR} values in Finland (Leskinen 2008). A large invasion of bird-cherry ermine moth (*Yponomeuta evonymellus*) was documented on a night with scattered showers; Z_{DR} values were readily differentiated between meteorological and biological echoes. Weak signal with $Z_{DR} > 1$ dB has been attributed to insects, given no wingbeats, small cross section, and low flight speed (Mueller and Larkin 1985).

Birds and insects can sometimes be differentiated using polarimetric radar variables—both exhibit very low copolar correlation coefficient values (0.3–0.5), indicating nonmeteorological scatter. Insects have high Z_{DR} (up to 10 dB) and relatively low differential phase, while birds may have lower Z_{DR} (-1 to 3 dB) and much larger differential phase (Zrnić and Ryzhkov 1998). Many echoes from birds have much higher Z_{DR} values, as shown below. Spectral analysis of the polarimetric radar signal may hold promise for distinguishing bioscatterers, perhaps to genus level in some cases (e.g., Bachmann and Zrnić 2007; Melnikov et al. 2010). As this technique requires level 1 radar data, however, it is unlikely to find widespread use in the near future.

Few studies discuss polarimetric characteristics of tropical cyclones (e.g., May et al. 2008; Shusse et al. 2009). To the author's knowledge, these and other studies do not note anomalies in the tropical cyclone eye region consistent with bioscatter. May et al. (2008) present a hydrometeor classification cross section extending across the eye of Australian tropical cyclone Ingrid (2005), which does not show bioscatter-consistent anomalies.

Observations of airborne organisms abound in tropical cyclones, particularly from when ship observations were routinely published. Airborne organisms are associated with the eyes of well-developed tropical cyclones, where they presumably become trapped as the eye is forming. After eye formation, many remain in the eye until it dissipates or moves over land, rather than seeking to escape through the eyewall convection. Prior observations have included mostly birds (e.g., General Weather Service of the United States 1882; Coronas 1925; Parry 1930; Hurd 1933), though reports of mixed birds and insects are also common (e.g., Young 1921; Hurd 1923, 1927; Tannehill 1936). At least one study includes observations of only insects—a large invasion of black witch moths (*Ascalapha odorata*), typically found in Mexico and southward, was reported on the central Texas coast associated with Hurricane Claudette (2003); this storm crossed the Yucatán Peninsula prior to landfall on the Texas coast (Freeman 2003).

The quantity and variety of airborne organisms reported in tropical cyclone eyes is remarkable. Ship reports have noted "the air was filled with thousands of birds and insects" (Young 1921, p. 358), and from a hurricane off the New England coast, "the center area was clearly defined by the presence of innumerable birds, land and shore birds of all sizes. . .more than 30 kinds of birds were counted, including an owl" (Mayhew 1949, p. 403). Birds of many sizes have been noted, ranging from "little reed birds to a large stork" (Garriott 1902, 473–474). Land and ocean birds have been noted; most reports of ocean birds are from land and most reports of land birds are from ships. Barring capture of migrating individuals, if land birds are present in the eye, then the tropical cyclone has passed over land at some prior point. Similarly, insects have often been observed in abundance, with a great variety of sizes represented. They include black witches (Freeman 2003) with a wingspan up to 15 cm, a ship ''literally covered with bugs'' (Hurd 1923, p. 475), and ''swarms of butterflies and moths'' (Tannehill 1936, p. 205). These observations are evidence that sufficient bioscatterers may be present in the eye of some tropical cyclones to appear in radar data. Characteristics of this bioscatter may lie somewhere between those associated with birds and insects.

Biological transport by tropical cyclones is not geographically isolated, but may occur whenever a tropical cyclone has a well-developed eye, whether or not it has passed over land. This phenomenon has been reported from the Gulf of Mexico (e.g., Parry 1930; Lowery 1946; Freeman 2003), New England and Newfoundland (e.g., Mayhew 1949; Tuck 1968), along the west coast of Mexico (e.g., Hurd 1927; Jones 1999; Webster et al. 1990), and in the west Pacific region (e.g., Hurd 1923; Coronas 1929; Hurd 1933; Doucette 1936). This unique mode of biological transport often brings unusual bird species to a region, especially ocean birds over land, particularly near the track of the eye after landfall. Examples of past biologically significant tropical cyclone transport include many ocean birds brought to Louisiana (Tannehill 1938) and Arizona (Jones 1999), laughing gulls (*Leucophaeus atricilla*) and black skimmers (*Rynchops niger*) in Newfoundland as a tropical cyclone eye was passing over (Tuck 1968; these species typically range much farther south), the first sooty tern (*Onychoprion fuscatus*) recorded in California (Webster et al. 1990), and an increase in magnificent frigatebirds (*Fregata magnificens*) over central Florida following tropical cyclones (McNair 2000). Tropical cyclones can substantially alter autumn migration over the Gulf of Mexico, possibly altering species distributions for several years (Thurber 1980). Polarimetric weather radar offers a powerful means to detect biological transport in tropical cyclones, with substantial value to biologists. Operational meteorologists should also be aware of the conspicuous signatures associated with biological transport, since they may be confused with precipitation.

Though bioscatter is typically associated with well-defined tropical cyclone eyes, it may also become focused near the center of a low-level wind circulation, as will be shown for Hurricane Sandy (2012). Bioscatter can also be caught up in the outer circulation. As a tropical cyclone approaches a coast, species from the near-coastal waters are often observed along the coast and inland, where the wind is blowing toward land (Kaufman 1977). Many of these species may also be transported by the eye of a tropical cyclone, but the presence of species spending most of their lives over the open ocean (pelagic species) and those typically occurring much farther south (particularly along the track of the tropical cyclone) are thought to be transported primarily by the eye.

In this paper, polarimetric radar observations of bioscatter will be presented from several recently upgraded WSR-88D radars. These observations will form a basis for identifying bioscatter in WSR-88D polarimetric radar data. Then, observations of biological transport in tropical cyclones will be presented for the first time, using Hurricanes Irene (2011) and Sandy (2012) as examples. The focus will be dual: 1) characteristics and evolution of the bioscatter signal will be discussed for the benefit of operational meteorologists; and 2) for Hurricane Irene, observations of anomalous species will be presented to lend credence to the interpretation of these signatures, and to provide biologists a baseline for comparing this storm's radar signatures with species observed at the surface.

2. Data and methods

Datasets are analyzed from the Morehead City, North Carolina, radar (KMHX; for Hurricane Irene) and the Mount Holly, New Jersey, radar (KDIX; for Hurricane Sandy). Radar data were displayed using the National Center for Atmospheric Research (NCAR) UNIDATA Interactive Data Viewer software, and radar data were obtained from the National Climatic Data Center archive. KMHX was fully upgraded to polarimetric capability on 28 June 2011, and captured the first operational polarimetric dataset of a tropical cyclone as Hurricane Irene swept up the coast in late August 2011. The focus of this study will be from 0000 UTC 27 August 2011, when the eye first appeared in the radar display, through landfall at approximately 1400 UTC 27 August, and ending at 1800 UTC 27 August when the eye became less distinct and had moved well away from the point of landfall. We will discuss the strength and areal coverage of the bioscatter signature as the eye moved by KMHX, and relate these observations to radar beam height. Potential data quality issues will be discussed relevant to signal interpretation. KDIX was fully upgraded to polarimetric capability on 31 January 2012. A less-detailed analysis of the KDIX data will be presented from 2200 to 0158 UTC 29–30 October 2012, when the post-tropical remnants of Hurricane Sandy made landfall on the southern New Jersey coast. Though this cyclone did not have a well-defined eye, its minimum central pressure (943 hPa) was consistent with

TABLE 1. Values of Z_{HH}, Z_{DR}, and ρ_{hv} in several types of biological scatter observed with the WSR-88D network, composite values representative of bioscatter, and values in scatter with similar radar appearance. Italicized values for sea clutter and light rain indicate substantial differences from the typical values associated with bioscatter.

Echo source	Radar	Z_{HH} (dB)	Z_{DR} (dB)	ρ_{hv}
Purple martins	KHTX	10–25	3–6+	0.5–0.8
Mexican free-tailed bats	KSJT	20–30	1.5–3	0.5–0.7
Nocturnally migrating birds	KICT	10–20	2–6+	0.5–0.7 (flying away)
				0.7–0.85 (flying toward)
Composite bioscatterer		<30	>2	0.5–0.8
	Reference			
Sea clutter	Ryzhkov et al. 2002	15–30	*−4 to 3* (textured)	0.2–0.5 (sometimes higher)
Light rain	Straka et al. 2000	<28	*0–0.7* (uniform)	*0.97+*

many category 3–4 hurricanes on the Saffir–Simpson scale, and a well-defined low-level circulation center appeared to trap many bioscatterers.

Bioscatter is identified and separated from similar signatures utilizing established values of the polarimetric variables for each scatterer type. Using additional polarimetric observations of several bioscatterer types, we have developed "composite" or typical values of the polarimetric variables associated with bioscatter from newly upgraded WSR-88D radars (Table 1). "Typical" values of the polarimetric variables in bioscatter were derived using several datasets. Purple martins were observed leaving a roost on the morning of 5 July 2012 by the Huntsville–Hytop, Alabama, WSR-88D (KHTX). The associated signal was characterized by low Z_{HH}, Z_{DR} higher than typically observed in meteorological echoes except very large raindrops, and ρ_{hv} lower than observed in meteorological echoes (Fig. 1; Table 1). Generally similar signatures were observed in scatter dominated by Mexican free-tailed bats seen from the San Angelo, Texas, WSR-88D (KSJT) on 7 July 2012 (not shown), and in a nocturnal bird migration observed over southern Kansas from the Wichita, Kansas, WSR-88D (KICT) on 4 November 2011. In the Kansas case (Fig. 2), bioscatter likely comprised many species, though the air temperature was sufficiently cold (−3° to 1°C) to preclude large-scale insect movement (also a frequent contributor to Great Plains bioscatter). In this case, ρ_{hv} varied by scatterer orientation. Birds flying away from the radar exhibited especially low ρ_{hv}, while birds flying toward the radar showed higher ρ_{hv} values approaching those expected in hail cores (0.7–0.85; Straka et al. 2000; Table 1). Compositing these three cases, bioscatter was generally characterized by $Z_{HH} < 30$ dBZ, $Z_{DR} > 2$ dB and often >3 dB, and ρ_{hv} between 0.5 and 0.8.

The operational polarimetric WSR-88D hydrometeor classification algorithm (HCA) contains a category for biological scatter (BS). This HCA works by assigning a probability, ranging from 0 to 1, to each of the 10 scatterer classifications for each of the four common polarimetric variables plus two texture parameters. Dominant scatterer type in a volume is identified as the type with the highest aggregated probability, modified by weighting factors (Park et al. 2009). The highest probability (1) is assigned to the BS category for $10 \le Z_{HH} \le 20$ dBZ, with some probability assigned down to 5 dBZ and up to 30 dBZ. The observations presented herein agree with this assessment, though Z_{HH} rarely reached up to 42 dBZ in Hurricane Irene during a time when bioscatterers were concentrated into a small area by convective development. The highest probability is also assigned to BS for $2 \le Z_{DR} \le 10$ dB and for $0.5 \le \rho_{hv} \le 0.8$ (Park et al. 2009). Our observations also agree with these ranges. In the WSR-88D HCA, echo is assigned a zero probability of being BS for $\rho_{hv} > 0.83$. We occasionally observed ρ_{hv} values of 0.85 in birds flying toward the radar. Overall, the operational HCA for the WSR-88D network appears to account reasonably well for the values of polarimetric variables observed in bioscatter as described herein.

Sea clutter, caused by the radar beam interacting with ocean waves, also typically has low Z_{HH} and very low ρ_{hv} (Table 1), though it can have ρ_{hv} values up to 0.99 (C. Van Den Broeke 2012, personal communication). It is distinguished by highly textured Z_{DR} with many substantial negative values. The Z_{DR} of bioscatter is typically uniformly high, with few or no negative values except sometimes in a defined lobe. Light rainfall is another source of radar echo, possibly mistaken for bioscatter in the tropical cyclone environment. It is distinguishable by its relatively low-magnitude positive Z_{DR} values and high ρ_{hv} (Table 1). Additionally, light rain may be distinguished from sea clutter by its relatively uniform, small positive Z_{DR} values, and by its very high ρ_{hv}. In this environment, therefore, scatterer identity is relatively well defined, including the distinction between bioscatter and light rainfall. Our focus is on polarimetric signatures associated with the eye of the tropical cyclone. The eye-associated bioscatter signature

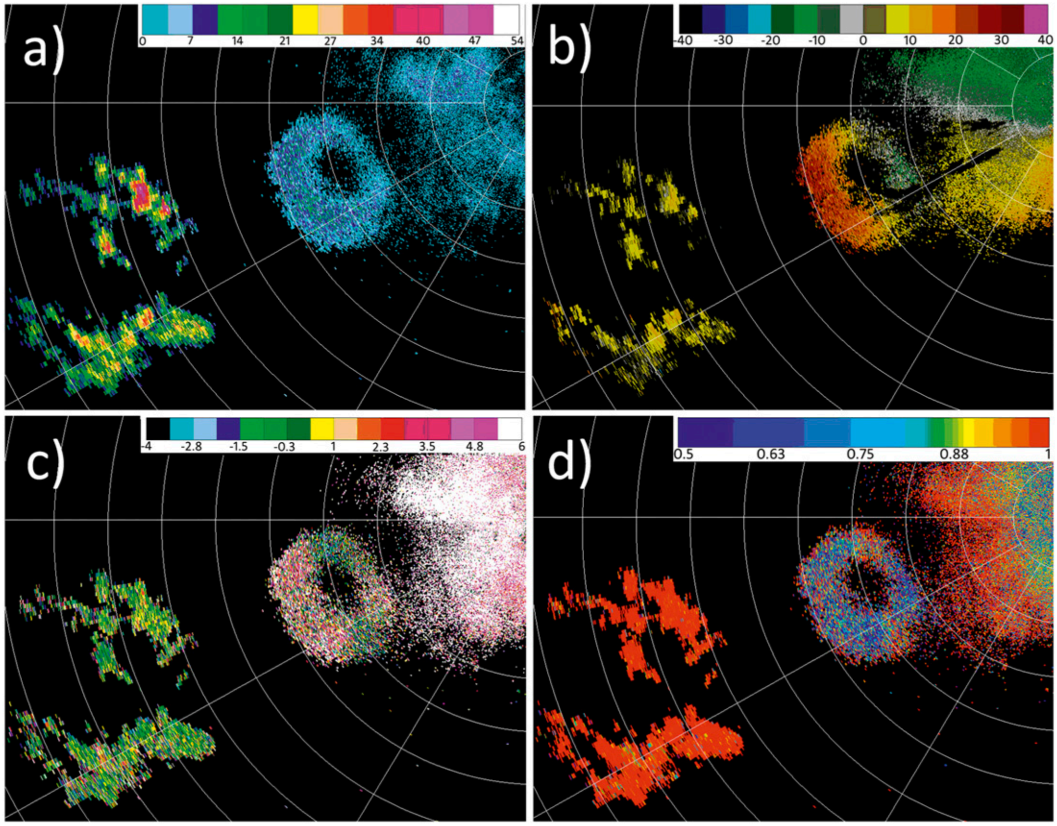

FIG. 1. Polarimetric radar signatures at a 0.5° elevation angle from KHTX at 1057 UTC 5 Jul 2012. Range rings every 25 km. (a) Values of Z_{HH} from 0 to 54 dBZ, (b) radial velocity (V_r) from −40 to +40 m s^{-1}, (c) Z_{DR} from −4 to 6 dB, and (d) ρ_{hv} from 0.5 to 1. Ring west of the radar corresponds to a dispersing roost of purple martins, and echoes near the west edge of the display correspond to an area of rain showers. Purple martins are characterized by relatively low Z_{HH}, high Z_{DR}, and low ρ_{hv}. (b) Shows the expanding nature of the ring.

remained consistent and persistent over land in Hurricanes Irene and Sandy, raising confidence that it was associated with bioscatter and not with return from ocean waves.

In conducting this analysis, we must consider whether high Z_{DR} values attributed to bioscatter are genuine. If not genuine, then a radar operator might observe high Z_{DR} values and erroneously associate them with bioscatter. In cases examined herein, the center of circulation typically consisted of mixed patches of rain, bioscatter, and weak echo. The Z_{HH} values in rain and bioscatter were often comparable, though Z_{HH} in bioscatter was occasionally larger than in nearby rain; Z_{HH} tended to be quite low in areas of weak echo (<2–5 dBZ). Despite similarities in Z_{HH}, rain and bioscatter contained very different Z_{DR} characteristics; Z_{DR} in rain was comparable to expectations for small drops (0–1 dB), while Z_{DR} in bioscatter was typically >6 dB and often up to 7.9 dB. Birds and insects are assumed to be prolate scatterers (e.g., Zrnić and Ryzhkov 1998), so these Z_{DR} values indicate horizontally oriented prolate scatterers. Such high Z_{DR} values were seen as Z_{HH} varied from 10 to 40 dBZ. *Observed ZDR values* in these regions *were consistently high and readily distinguishable* from those in nearby rain. Thus, these echoes can be attributed with high confidence to bioscatter.

For Hurricane Irene, constant altitude plan position indicator (CAPPI) slices were made across the eye region at 500, 1000, 1250, 1500, and 1800 m. CAPPIs were prevented from showing 0.5° elevation angle data to the edge of the domain. To accomplish this, the maximum range of the 0.5° data was calculated for the five CAPPI levels using the standard 4/3 Earth radius model (Doviak and Zrnić 1993), valid for beam centerline:

$$\text{Radar beam height} = \sqrt{r^2 + a_e^2 + 2ra_e\sin(\theta_e)} - a_e\,,$$

where r is the range to the center of the bioscatter signature, a_e equals 4/3 the radius of the earth (6.495×10^6 m), and θ_e is the radar elevation angle. Only times when the bioscatter signature was fully within the

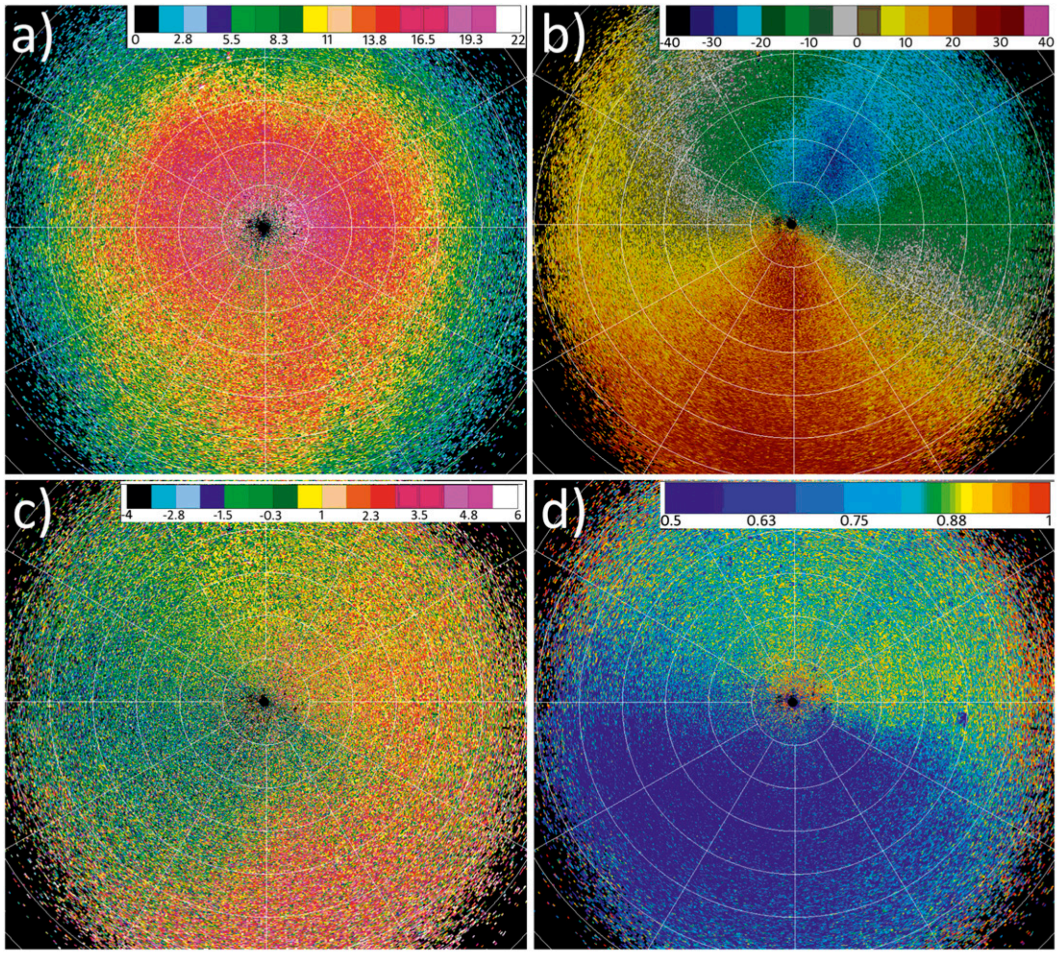

FIG. 2. As in Fig. 1, but for KICT at 0405 UTC 4 Nov 2011. Range rings every 20 km. (a) Values of Z_{HH} from 0 to 22 dBZ. Large area of light echo around the radar corresponds to nocturnally migrating birds, on a night with light north winds. Migrating birds are traveling generally south, as indicated in (b), and are characterized by relatively low Z_{HH}, high Z_{DR}, and ρ_{hv} that is low everywhere but lowest where birds are flying away from the radar.

maximum range were included in the analysis. This equation assumes a linear relationship between refractive index and height, and performs poorly when a vertical temperature discontinuity is present. Generally this equation has been found to perform well in the lowest 1–2 km. The bioscatter signal in Hurricane Irene was concentrated at <1.5 km in depth. This and the small distance traveled by the radar beam through the eye where sharp vertical temperature discontinuities may occur increase confidence that this method provides a reasonable estimate of beam height. This, in turn, yields high confidence that our choice of times for CAPPI analysis should yield representative results.

Altitude of the bioscatter signature was also estimated using the 4/3 Earth radius model. The validity of this equation varies with distance from the radar, since the radar beam broadens with distance. This model gives an estimated height of *beam centerline* for a given range. Given the 1° WSR-88D 3-dB beamwidth, the beam at $r = 100$ km has a vertical spread of 1.7 km. In addition, scatterers in the main lobe yet outside of the 3-dB beamwidth may be a weak source of power return. It is thus important to note that all bioscatter altitudes reported herein are valid for beam centerline and may contain considerable error.

Maximum Z_{HH} within the bioscatter signal was recorded for each analysis time. Areal extent of the bioscatter signature was then estimated by assuming it covered a partial annulus, the area of which was calculated using

$$\text{Areal extent} = \pi(R^2 - r^2)\frac{\theta}{360°},$$

where (R, r) represent range to the outer and inner boundaries of the partial annulus, respectively; and

θ is the azimuthal angle subtended by the bioscatter signature.

Ground observations of anomalous bird species associated with Hurricane Irene were gathered from ornithological publications (e.g., Williams 2011; Southern 2011; Mitra 2011; Yandik 2011; Bochnik 2011; Lindsay and Mitra 2011). These species were sorted to represent those typically associated with nearshore waters, and pelagic species or species typically living well south of where they were observed (procedure described in section 4b). A list of latitude–longitude points was developed to represent each sighting, and these were plotted with the National Hurricane Center's (NHC's) best track for Hurricane Irene.

3. Overview of Hurricane Irene (2011) and Hurricane Sandy (2012)

Hurricane Irene (2011) was the first well-structured tropical cyclone to make landfall within the domain of an operational polarimetric WSR-88D weather radar. A strong tropical wave that would become Irene exited the African coast on 15 August, and a low-level circulation became evident on 20 August. The system reached St. Croix on 21 August with sustained winds near 60 kt ($1\,\mathrm{kt} = 0.51\,\mathrm{m\,s^{-1}}$). Irene continued northwest toward Puerto Rico (Fig. 3a), where it made landfall on 22 August. It became a hurricane shortly thereafter, and was briefly a major hurricane on 24 August. Irene's sustained winds began to weaken, and by landfall at Cape Lookout, North Carolina, around 1200 UTC 27 August, sustained winds were only 75 kt. The storm maintained a remarkably low central pressure (952 hPa) through its North Carolina landfall, however, possibly explaining the well-defined eye still present. The relative coherence of the inner core structure as Irene moved inland may be partially responsible for the large number of oceanic bird species reported well inland along Irene's track. Irene continued moving north-northeast and tracked over New England (Fig. 3a), with additional landfalls at Brigantine Island, New Jersey (0935 UTC 28 August; 959 hPa) and Coney Island, New York (1300 UTC 28 August; 965 hPa). The system became extratropical near the border of Vermont and New Hampshire around 0000 UTC 29 August, and continued north into Canada.

Hurricane Sandy (2012) formed off the coast of northern South America and then tracked north over eastern Cuba and the Bahamas. North of the Bahamas, the system paralleled the U.S. coast to latitude 35°N. A strong trough in the polar jet stream approached from the west, and interaction between the two centers of vorticity caused Sandy to turn sharply westward while transitioning away from a purely tropical state. The cyclone became post-tropical and made landfall near Atlantic City, New Jersey, around 0000 UTC 30 October 2012. It rapidly weakened while affecting much of New England with heavy rainfall for several days.

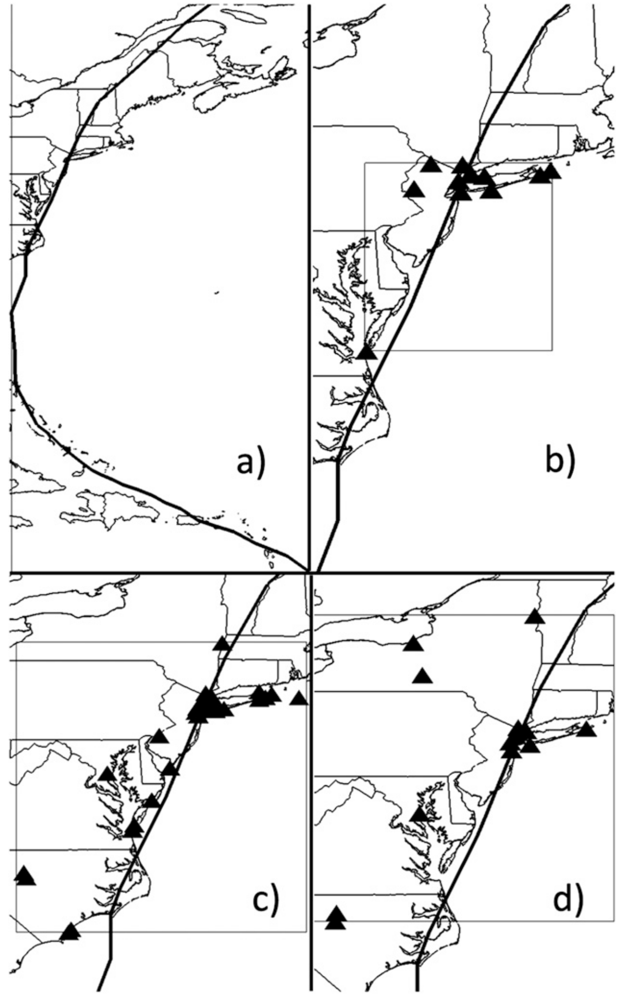

FIG. 3. Track of Hurricane Irene (2011) relevant to this study. (a) Locations of anomalous bird species noted with the passage of Irene indicated as black triangles in remaining panels. (b) Irene-associated reports of bird species typically ranging in the tropics and subtropics well south, and with high probability of having been transported in the tropical cyclone's eye. (c) Irene-associated reports of bird species typically located well offshore but at the latitude of the report; these species were possibly transported in Irene's general wind field. (d) Irene-associated reports of bird species that are often present near the location of the report, but which were noted as anomalous in discussions of sightings from Irene.

4. Observations of biological scatterers

a. Hurricane Irene (2011)

A bioscatter-consistent signature first appeared in Hurricane Irene at the 0.5° elevation angle at approximately

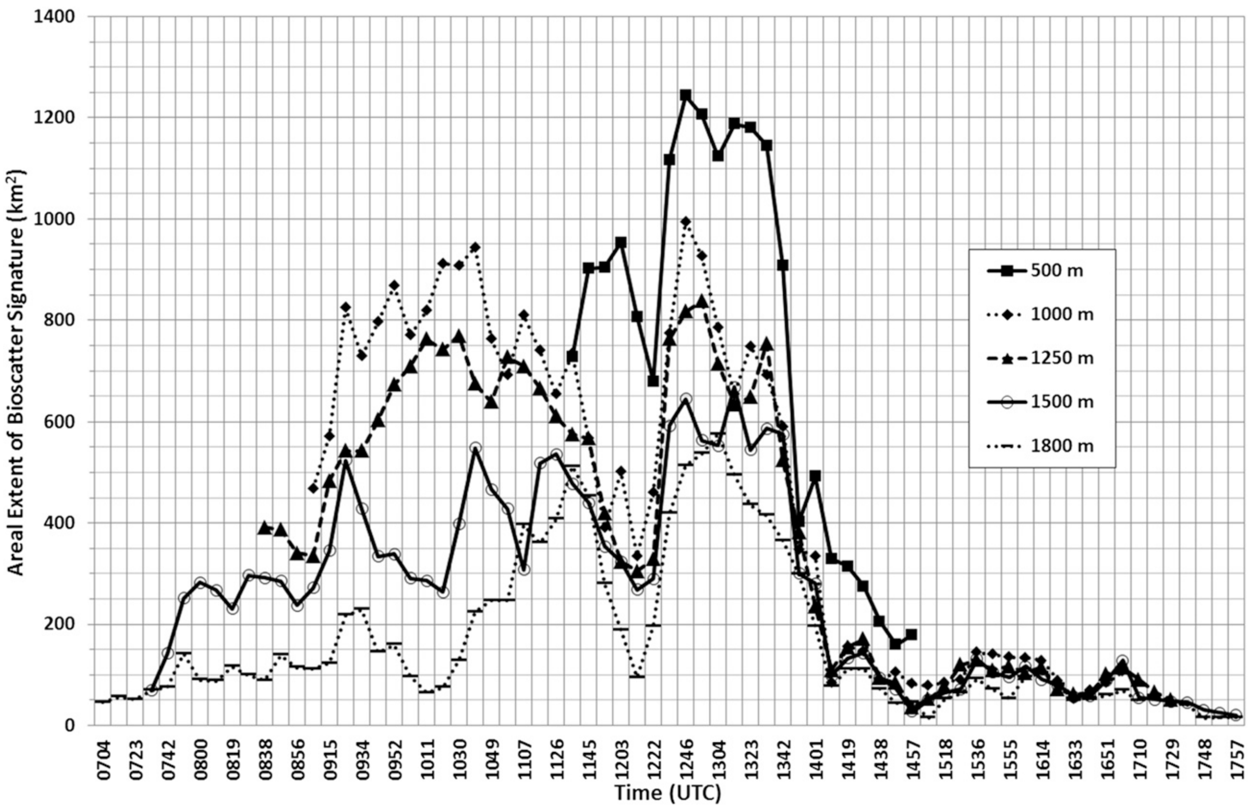

FIG. 4. Areal coverage (km^2) of the polarimetric radar signature consistent with bioscatter for chosen CAPPI levels. Decrease in areal coverage, most notable around 1215 UTC, is consistent with convective development in the eye, while significant decline beginning just prior to 1400 UTC is associated with landfall.

0704 UTC, at a range of 110 km. Using the 4/3 Earth radius model of beam propagation, this corresponds to a beam centerline at an altitude of ~1.7 km. CAPPIs of 1800 and 1500 m consistently contained bioscatter through 1757 UTC, with peak areal signal extent from 1300 to 1330 UTC (Fig. 4).

Areal coverage of the bioscatter signature fluctuated moderately once the eye of Irene was within ~75 km of the radar at 0920 UTC (Fig. 4). It filled much of the eye and was associated with characteristic high Z_{HH} and low ρ_{hv} values (Fig. 5; 1103 UTC). A sharp decrease in areal coverage was apparent at nearly every CAPPI level centered on approximately 1215 UTC. The onset of this decline around 1149 UTC was marked by development of several convective clusters in the eye, splitting the bioscatter signature into two distinct areas. Areal extent of the signature reached a relative minimum around 1208 UTC (Fig. 6) and then increased afterward as convection diminished in the eye (Fig. 4). These observations suggest the region of bioscatter may readily conform to the shape of the eye, given that birds dominate the bioscatter signal and will seek to avoid eyewall convection and any convection within the eye. Such active flying, sustained in some cases over many days, would explain the exhaustion often exhibited by birds observed in tropical cyclone eyes (e.g., Hurd 1933). Immediately prior to and following Irene's eye making landfall around 1400 UTC, areal extent of the bioscatter signature rapidly decreased at all CAPPI levels (Fig. 4). A substantial area of bioscatter remained in the eye as it moved inland over North Carolina, becoming too far from the radar to be readily visible by 1800 UTC. The decrease after landfall is consistent with birds descending toward the surface as soon as land was visible, since these birds may have been in flight for a long period of time and would want rest. Part of the signature decrease may also represent insects descending toward the surface. This possibility should be considered in future work, along with how signature changes may relate to the diurnal activity cycle of some insect species.

Areal coverage of the bioscatter signature generally decreased with height (Fig. 4). This is expected, given that most bird species would not expend energy to fly to great altitudes. Coverage was often much greater in the 500-m CAPPI than at any other vertical level examined, with smaller differences between vertical levels after

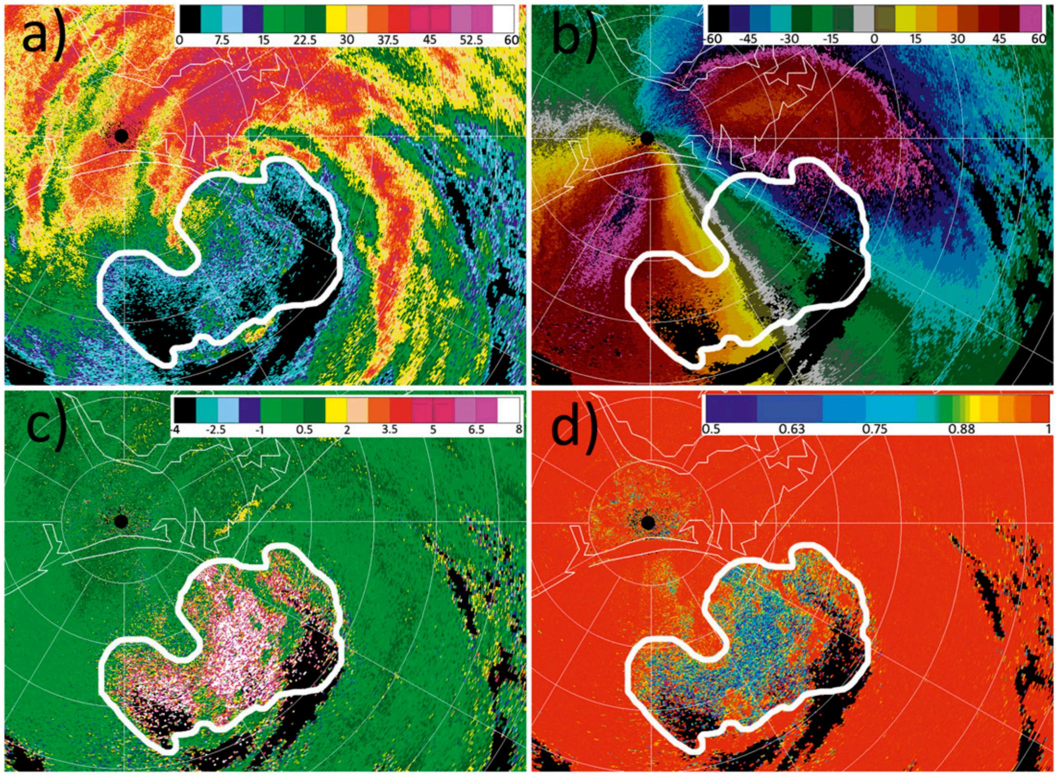

FIG. 5. Example of 0.5° bioscatter signature in Hurricane Irene at 1103 UTC, a time of large signature areal coverage. Range rings every 20 km. (a) Values of Z_{HH} from 0 to 60 dBZ, (b) V_r from -60 to $+60\,\mathrm{m\,s^{-1}}$, (c) Z_{DR} from -4 to 7.9 dB, and (d) ρ_{hv} from 0.5 to 1. Bioscatter signature associated with the eye of Irene clearly appears as an area of (c) high Z_{DR} and (d) low ρ_{hv} The white outline roughly encloses the area of bioscatter.

Irene's landfall. Areal extent of the bioscatter signature was especially large at 500 m compared to the other vertical levels around 1215 UTC, when convection was ongoing in the eye. Sufficient coverage was present in higher-elevation CAPPIs to preclude sea clutter or sea spray contamination. Areal extent in the 1800 m CAPPI appeared to be reduced from ~(1000–1030) UTC because of the choice of levels used in CAPPI calculation.

Radial velocity values are typically not significantly different in the region of bioscatter (Figs. 5, 6). While this may indicate mostly insects that would advect with the background flow rather than strongly flying, the high reflectivity values in these regions (20–40+ dBZ) indicate many birds are likely present, especially given the lack of observations of significant insect arrival when Hurricane Irene made landfall. Very strong background flow may diminish the likelihood of seeing a velocity signature distinct from surroundings in areas of bioscatter.

Maximum altitude of the bioscatter signature can be compared with inversion height in Irene's eye. This comparison presents challenges, given the scarcity and coarse vertical resolution of representative data. This is a valuable comparison, however, since inversion height is a function of several thermodynamic processes ongoing in and near the cyclone core (Willoughby 1998), which may be of use once we more clearly understand the relationship between inversion height and tropical cyclone intensity.

Dropsonde observations from Irene's eye are available from 0749, 0913, 1023, and 1119 UTC. Resolution was coarse, with each dropsonde profile containing only four to six observations in the surface to the 700-hPa layer. High-density observations are available from National Oceanic and Atmospheric Administration (NOAA) and U.S. Air Force reconnaissance flights, though these flights stayed around 750 and 700 hPa, respectively, so are of little value in determining inversion height. The routine 1200 UTC sounding from KMHX (not shown) indicated a 22-kt north wind and a surface pressure of 962 hPa, so it was not close enough to the eye to judge inversion height. Indeed, a well-defined inversion was not present. Radar data from this time show KMHX was located on the east edge of the reflectivity gradient associated with the eyewall, so this sounding likely captured conditions at the edge of the eyewall rather than those truly representative of the eye.

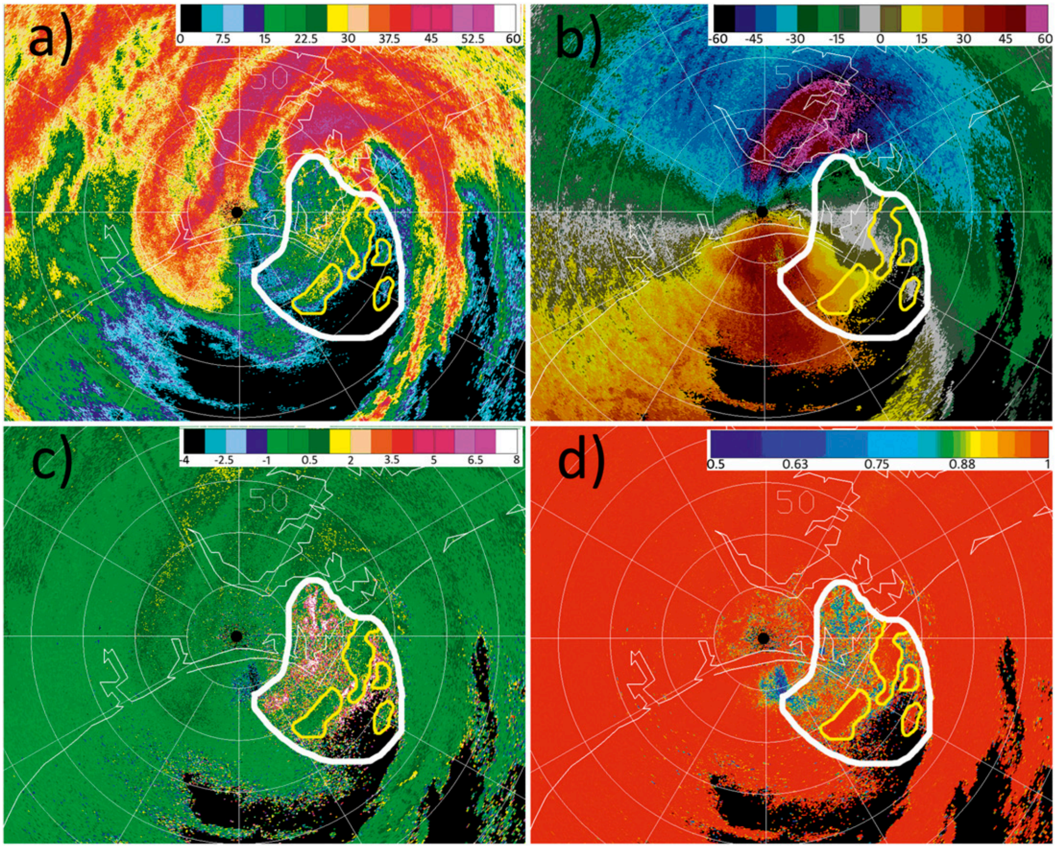

FIG. 6. Polarimetric signatures associated with convection in the eye of Hurricane Irene at 1208 UTC (0.5° elevation angle). Panels and range rings as in Fig. 5. The areal extent of bioscatter (roughly outlined in white) reached a relative minimum around this time, attributed to deep convection present in the eye (outlined in yellow).

Dropsonde data did not clearly indicate an inversion at 0913 and 1119 UTC. At 0749 and 1023 UTC, a moist layer near the surface abruptly terminated with a sharp increase in dewpoint depression (DD) above—this DD increase was taken to mark the inversion (e.g., Willoughby 1998). In both cases, the level of drying also corresponded to a nearly isothermal layer, though the temperature below had decreased with height (Table 2). At 0749 UTC, the inversion was between 789 hPa (DD = 0.6°C) and 755 hPa (DD = 2.8°C). Elevations of these pressures are not available from the dropsonde data. The KMHX sounding, though four hours separated from this dropsonde data, through direct comparison of pressure would yield an inversion height of 1.8–2.1 km. At this time, the highest-altitude bioscatter signature was observed on the 0.9° elevation angle scan at ~2.1 km, in good agreement with this estimate of inversion height. By 1023 UTC, the inversion was between 850 hPa (DD = 0.4°C) and 804 hPa (DD = 2.6°C; Table 2). The 850-mb height of 997 m is approximately 100 m lower than the value from the KMHX sounding two hours later. Applying a crude 100-m correction, inversion height at 1023 UTC is estimated at 1.1 km, though potential error of this estimate is large. Regardless, the inversion height appears to have dropped substantially between 0749 and 1023 UTC. By 1025 UTC, the maximum altitude of the bioscatter signature was estimated at 1.4 km. Thus, an apparent decrease in inversion height from 0749 to 1023 UTC was also associated with a decrease in the height at which the bioscatter signature was observed. With further observations, it may be possible to use the bioscatter signature to estimate inversion height changes in tropical cyclones, given a well-defined eye.

Signal strength and ''goodness of match'' of the observed signature to expected characteristics of bioscatter were considered. Of the polarimetric variables, Z_{DR} most obviously differentiated the signature of interest—uniform values > 6 dB were common, and values were often uniformly 7.9 dB (the cap on WSR-88D-reported Z_{DR} values). The value of ρ_{hv} was typically less than 0.6 in areas dominated by bioscatter, though values increased to 0.85–0.9 where the bioscatter signature overlapped light precipitation. Reflectivity in regions of bioscatter reached a maximum of 35–40 dBZ at 0.5° for

TABLE 2. Dropsonde data from Irene's eye, from 0749 and 1023 UTC. N/A indicates the particular parameter was missing at that vertical level. The inversion, identified by a sudden increase in dewpoint depression with height, is between the two bolded levels at each time.

Pressure (hPa)	Temperature (°C)	Dewpoint Depression (°C)	Height (m)
0749 UTC			
952	27	0.2	0
925	25.8	0.2	256
850	22.8	0.4	1002
789	**19.8**	**0.6**	**N/A**
755	**19.8**	**2.8**	**N/A**
716	17.2	1.9	N/A
1023 UTC			
951	27.4	0.6	0
925	26.2	0.7	251
850	**22.8**	**0.4**	**997**
804	**22.7**	**2.6**	**N/A**
700	N/A	N/A	2679

TABLE 3. Bird species included in each of the three categories (refer to text).

Anomalous bird species associated with Hurricane Irene (2011)	
Category A: Significant latitudinal transport	
Brown-chested martin	*Progne tapera*
Sooty tern (north of 40°)	*Onychoprion fuscatus*
White ibis (north of 40°)	*Eudocimus albus*
Category B: Significant longitudinal transport	
Pomarine jaeger	*Stercorarius pomarinus*
Wilson's storm-petrel	*Oceanites oceanicus*
Band-rumped storm-petrel	*Oceanodroma castro*
White-faced storm-petrel	*Pelagodroma marina*
Black-capped petrel	*Pterodroma hasitata*
South polar skua	*Stercorarius maccormicki*
White-tailed tropicbird	*Phaethon lepturus*
Bridled tern	*Onychoprion anaethetus*
Sooty tern (south of 40°)	*Onychoprion fuscatus*
Category C: No significant transport necessary; noted as anomalous	
Long-tailed jaeger	*Stercorarius longicaudus*
Leach's storm-petrel	*Oceanodroma leucorhoa*
Laughing gull	*Leucophaeus atricilla*
Great shearwater	*Puffinus gravis*
Least tern	*Sternula antillarum*
Common tern	*Sterna hirundo*
Royal tern	*Sterna maxima*
Caspian tern	*Hydroprogne caspia*
Sandwich tern	*Thalasseus sandvicensis*

~50 min centered on 1200 UTC. This corresponded to a decrease in bioscatter signature areal extent because of convection, suggesting scatterers were indeed more concentrated. Reflectivity decreased with altitude, suggesting lower scatterer concentration with increasing altitude.

b. *Ground observations of anomalous bird species during Hurricane Irene*

Many sightings of unusual bird species associated with Irene were published in the ornithological literature, which was examined for reports of typically oceanic species as the center of Irene passed by. When an unusual species was noted, Google Maps was used to estimate a latitude–longitude for the sighting, generally accurate to within 0.01°. Many valuable sightings did not have a sufficiently detailed location and were discarded. Once a list of reported species was compiled, range maps from the NatureServe project (Ridgely et al. 2003) were studied to classify species by their typical region of occurrence. *Category A species* typically live in the tropics or well south of the latitude of report during Irene. These species would have been carried a substantial *latitudinal distance* by Irene, and were considered most likely to have been transported by Irene's eye. *Category B species* were pelagic, typically occurring well offshore and not likely to be seen near land. These species would have been transported a substantial *longitudinal distance* by Irene. Given their usual occurrence at high latitude, however, these species are not necessarily transported by the eye, but may be transported by the general wind field. *Category C species* live along the coast and sometimes well inland, but were noted as out of place during Irene. These species were possibly blown off course during migration, but may not have been transported any significant distance by the hurricane. Species in each classification are noted in Table 3.

Latitude–longitude points of observations in each category were plotted with the track of Irene. Category A species, those transported a substantial latitudinal distance, were observed closer to the track of the circulation center than other categories (Fig. 3b). These species were also observed nearer to the coast than species in the other categories. Sooty tern, in particular, was frequently observed near the population center of New York City. Observations of these species near the coast and near the track of the circulation center represent evidence that they may have constituted some of the observed bioscatter signature in Irene, though other species were also almost certainly present. Observed spread of these species from the track of the circulation center could represent dispersal after leaving the center of circulation, or could reflect the less well-defined center of circulation as Irene traveled north along the coast.

Observations of category B species, those transported a substantial longitudinal distance, exhibited more spread around the track of the circulation center, with some observations as far west as central North Carolina and some as far east as the longitude of eastern

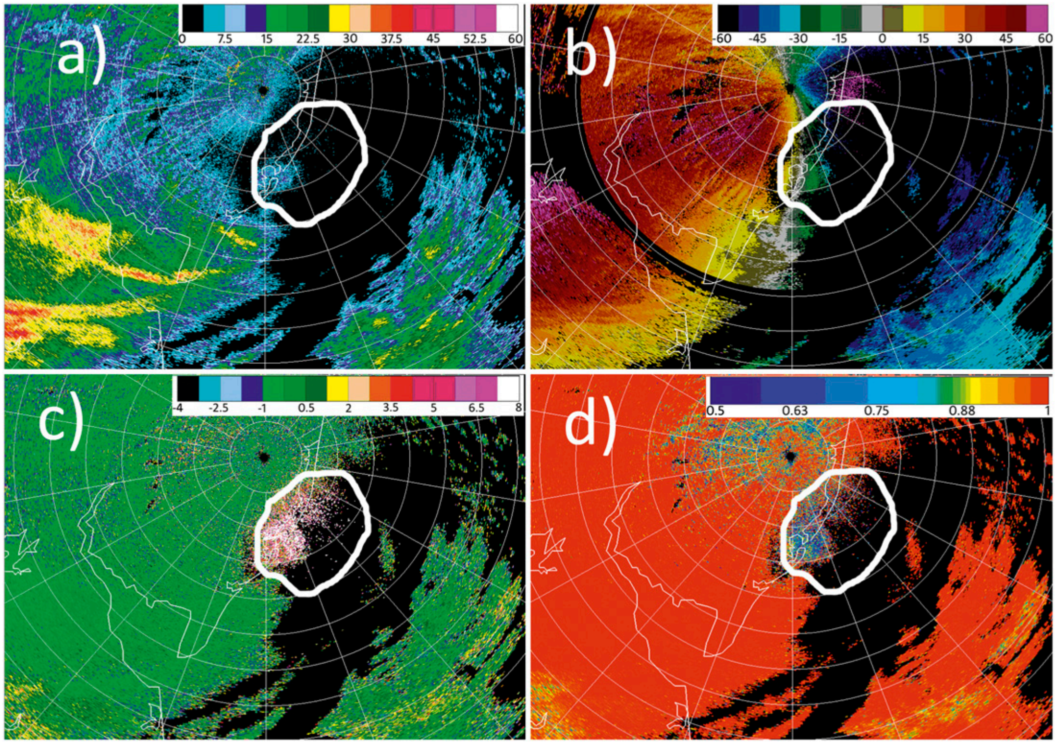

FIG. 7. Example of 0.5° bioscatter signature in Hurricane Sandy at 2341 UTC 29 Oct, near the time when the bioscatter signature and center of circulation made landfall. Panels and range rings as in Fig. 5. Bioscatter signature associated with the circulation center of Sandy clearly appears as an area of (c) high Z_{DR} and (d) low ρ_{hv} in near the coast, and is roughly outlined in white.

Connecticut (Fig. 3c). One major limitation is the lack of ornithological data from Delaware, Pennsylvania, Connecticut, Rhode Island, Massachusetts, and states north. Thus, the true extent of these species is likely underestimated. Greater deviation from the track of Irene is expected with these species, since they are more likely to have been transported in the easterly wind field to Irene's north. These species are not, however, precluded from transport by the eye. A population bias is again evident around New York City, but the available observations suggest a relatively uniform distribution of these species along the track of Irene.

Observations of category C species, those often present in the region but noted as unusual in ornithological reports from Irene, exhibited much greater spread about the track (Fig. 3d). Reports from New York indicate a wide scattering of these species statewide, indicating possible displacement of southward-migrating species in the wind field north of Irene.

c. *Hurricane Sandy (2012)*

The bioscatter signature in Hurricane Sandy was more short lived, appearing around 2200 UTC 29 October and disappearing by 0158 UTC 30 October. At first appearance at 0.5°, the signature was located about 120 km south-southeast of KDIX, which is comparable to the range at which the signature first appeared in Irene. The bulk of 0.5° bioscatter signal areal coverage arrived at the southern New Jersey coast around 2341 UTC (Fig. 7), in agreement with the NHC's assessment of landfall around 0000 UTC near Atlantic City, New Jersey. At this time, the signature was present 10–20 km south of KDIX up to an elevation of 1.5–2.2 km. Shortly after landfall, the signature merged with a region of ground clutter just inland over southern New Jersey, but emerged 20 minutes later to the west of the ground clutter. By 0032 UTC, Z_{HH} magnitude was decreasing in the bioscatter signal; this trend continued until the signal disappeared around 0200 UTC. Prior to significant signal weakening, the bioscatter signature at 0.5° reached up to 60 km inland. The Z_{HH} values through Sandy were typically not as high as those observed during Hurricane Irene, though values up to 20 dBZ were occasionally observed prior to landfall.

5. Conclusions and discussion

The new application of radar observations to detect bioscatter in tropical cyclones, described herein, is useful for meteorologists and biologists. Meteorologists should be aware of the radar bioscatter signature near the circulation center of tropical or strong post-tropical cyclones. It may appear similar to light precipitation in the eye, particularly at lower elevation angles, but has unique polarimetric characteristics of uniformly high Z_{DR} (4–7.9 dB) and low ρ_{hv} (0.3–0.8). This signature typically appears first at the lowest tilt, when distance to the circulation center is 100–120 km. It becomes visible in successively higher tilts as the center of circulation approaches the radar, possibly becoming visible to an elevation angle of 8° if the circulation center is within 30 km of the radar. The signature may be more visible at higher tilts if the circulation center is enclosed by an eyewall, and may change markedly in areal extent depending on the distribution of convection in the eye. The highest elevation at which the bioscatter signature appears may approximately mark the inversion height within the eye, though this conclusion warrants further research. If true, then the bioscatter signature may be a way to monitor temporal inversion height changes, which may in turn be relevant to thermodynamics associated with system intensity changes.

Biologists may also find the bioscatter signature useful. Some past tropical cyclones were noted for their significant biological transport, though there was no way to assess this transport prior to landfall (barring ship observations). The bioscatter signature may provide a means to identify in advance particularly significant storms in terms of biological transport. Though this transport appears to represent primarily birds in cases observed thus far, significant transport of insects has also occurred and should be detectable. Such biological transport may occasionally introduce a pest species (e.g., Leskinen et al. 2009) or a species not yet occurring in an affected region. Future study on this signature may provide a way to estimate bioscatter mass flux. Weather radar data in being applied more commonly to study biological questions, and polarimetric radar data in particular, offer a promising source of applications to bird migration, insect movements, bat behaviors, and biological transport by weather systems.

Building a holistic understanding of biological scatter in tropical cyclones is a difficult challenge, requiring the input of atmospheric scientists, remote sensing experts, ornithologists, and entomologists. Future work will require coordinated observations on several scales. The bioscatter signature should also be sought in strong coastal cyclones (nor'easters) to see if a strong circulation is sufficient to trap bioscatterers near its center, or if a tropical-type cyclone is essential. The differing seasonal and geographic distributions of various species must also be considered in such studies. Such research holds significant potential to help meteorologists interpret radar observations near the center of strong circulations, and to help biologists estimate bioscatter transport in cyclone wind fields.

Acknowledgments. The lead author was supported by an academic appointment at the University of Nebraska–Lincoln. Cynthia Van Den Broeke is acknowledged for contributions to study design and organization. Kent Fiala, Shaibal Mitra, and Bill Williams are acknowledged for providing access to ornithological data. Adam Houston, Curtis Walker, Amanda Wekesser, and Kun-Yuan Lee are acknowledged for their helpful comments on the manuscript. Three peer reviewers provided excellent comments, which significantly strengthened the manuscript.

REFERENCES

Achtemeier, G. L., 1991: The use of insects as tracers for ''clear-air'' boundary-layer studies by Doppler radar. *J. Atmos. Oceanic Technol.,* **8,** 746–765.

Bachmann, S., and D. Zrnić, 2007: Spectral density of polarimetric variables separating biological scatterers in the VAD display. *J. Atmos. Oceanic Technol.,* **24,** 1186–1198.

Bochnik, M., 2011: Region 9—Hudson-Delaware. *Kingbird,* **61,** 357–361.

Bonter, D. N., S. A. Gauthreaux, and T. M. Donovan, 2009: Migrating birds: Remote sensing with radar in the Great Lakes Basin. *Conserv. Biol.,* **23,** 440–448.

Bringi, V. N., and V. Chandrasekar, 2001: *Polarimetric Doppler Weather Radar: Principles and Applications.* Cambridge University Press, 636 pp.

Chapman, J. W., V. A. Drake, and D. R. Reynolds, 2011: Recent insights from radar studies of insect flight. *Annu. Rev. Entomol.,* **56,** 337–356.

Chilson, P. B., W. F. Frick, P. M. Stepanian, J. R. Shipley, T. H. Kunz, and J. F. Kelly, 2012a: Estimating animal densities in the aerosphere using weather radar: To *Z* or not to *Z*? *Ecosphere,* **3,** Article 72, doi:10.1890/ES12-00027.1.

——, and Coauthors, 2012b: Partly cloudy with a chance of migration: Weather, radars, and aeroecology. *Bull. Amer. Meteor. Soc.,* **93,** 669–686.

Coronas, J., 1925: Only one shallow depression and one small, but intense, typhoon over the Philippines in October, 1925. *Mon. Wea. Rev.,* **53,** 456–457.

——, 1929: Typhoons and depressions in November, 1929. *Mon. Wea. Rev.,* **57,** 525–526.

Diehl, R. H., R. P. Larkin, and J. E. Black, 2003: Radar observations of bird migration over the Great Lakes. *Auk,* **120,** 278–290.

Doucette, B. F., 1936: Typhoons and depressions over the Far East, October 1936. *Mon. Wea. Rev.,* **64,** 344–345.

Doviak, R. J., and D. S. Zrnić, 1993: *Doppler Radar and Weather Observations.* Academic Press, 562 pp.

Freeman, B., 2003: A fallout of black witches (*Ascalapha odorata*) associated with Hurricane Claudette. *News of the Lepidopterists' Society,* No. 3, Lepidopterists' Society, Round Rock, TX, 71.

Frick, W. F., P. M. Stepanian, J. F. Kelly, K. W. Howard, C. M. Kuster, T. H. Kunz, and P. B. Chilson, 2012: Climate and weather impact timing of emergence of bats. *PLoS ONE,* **7,** e42737, doi:10.1371/journal.pone.0042737.

Garriott, E. B., 1902: Forecasts and warnings. *Mon. Wea. Rev.,* **30,** 473–474.

Gauthreaux, S. A., and C. G. Belser, 1998: Displays of bird movements on the WSR-88D: Patterns and quantification. *Wea. Forecasting,* **13,** 453–464.

General Weather Service of the United States, 1882: Introduction. *Mon. Wea. Rev.,* **10** (9), 1.

Horn, J. W., and T. H. Kunz, 2008: Analyzing NEXRAD Doppler radar images to assess nightly dispersal patterns and population trends in Brazilian free-tailed bats (*Tadarida brasiliensis*). *Integr. Comp. Biol.,* **48,** 24–39.

Hurd, W. E., 1923: North Atlantic Ocean. *Mon. Wea. Rev.,* **51,** 474–476.

——, 1927: North Pacific Ocean. *Mon. Wea. Rev.,* **55,** 430–431.

——, 1933: North Pacific Ocean, September 1933. *Mon. Wea. Rev.,* **61,** 283–284.

Jones, R., 1999: Seabirds carried inland by Tropical Storm Nora. *West. Birds,* **30,** 185–192.

Kaufman, K., 1977: The changing seasons: An intimate look at Kathleen and other avian phenomena of autumn, 1976. *Amer. Birds,* **31,** 142–152.

Lakshmanan, V., J. Zhang, and K. Howard, 2010: A technique to censor biological echoes in radar reflectivity data. *J. Appl. Meteor. Climatol.,* **49,** 453–462.

Leskinen, M., 2008: Observed polarimetric signals of insects. *Proc. Fifth European Conf. on Radar in Meteorology and Hydrology,* Helsinki, Finland, Finnish Meteorological Institute, 2.3.

——, and Coauthors, 2009: Pest insect immigration warning by an atmospheric dispersion model, weather radars and traps. *J. Appl. Entomol.,* **135,** 55–67.

Lindsay, P. J., and S. S. Mitra, 2011: Region 10—Marine. *Kingbird,* **61,** 362–370.

Lowery, G. H., 1946: Evidence of trans-gulf migration. *Auk,* **63,** 175–211.

May, P. T., J. D. Kepert, and T. D. Keenan, 2008: Polarimetric radar observations of the persistently asymmetric structure of tropical cyclone Ingrid. *Mon. Wea. Rev.,* **136,** 616–630.

Mayhew, J. R., 1949: Atmospheric pressure and bird flight. *Science,* **109,** 403.

McNair, D., 2000: The status of magnificent frigatebirds in the interior of Florida. *North Amer. Birds,* **54,** 11–15.

Melnikov, V., M. Leskinen, and J. Koistinen, 2010: Spectral polarimetric parameters of radar signals from atmospheric biota. *Proc. Sixth European Conf. on Radar in Meteorology and Hydrology,* Sibiu, Romania, ERAD, P10.8. [Available online at http://www.erad2010.org/pdf/POSTER/Wednesday/04_Others/09_ERAD2010_0208_extended_modificat.pdf.]

Mitra, S. S., 2011: Tropical Storm Irene in New York State. *Kingbird,* **61,** 293–298.

Mueller, E. A., and R. P. Larkin, 1985: Insects observed using dual-polarization radar. *J. Atmos. Oceanic Technol.,* **2,** 49–54.

O'Neal, B. J., J. D. Stafford, and R. P. Larkin, 2010: Waterfowl on weather radar: Applying ground-truth to classify and quantify bird movements. *J. Field Ornithol.,* **81,** 71–82.

Park, H., A. V. Ryzhkov, D. S. Zrnić, and K.-E. Kim, 2009: The hydrometeor classification algorithm for the polarimetric WSR-88D: Description and application to an MCS. *Wea. Forecasting,* **24,** 730–748.

Parry, B., 1930: Appendix I.—Storm conditions encountered by the steamship ''Coamo'' September 3, 1930. *Mon. Wea. Rev.,* **58,** 363.

Ridgely, R. S., T. F. Allnutt, T. Brooks, D. K. McNicol, D. W. Mehlman, B. E. Young, and J. R. Zook, 2003: Digital distribution maps of the birds of the Western Hemisphere, version 1.0. NatureServe, 6 pp. [Available online at http://www.natureserve.org/library/birddistribmapsproject.pdf.]

Russell, K. R., D. S. Mizrahi, and S. A. Gauthreaux, 1998: Large-scale mapping of purple martin pre-migratory roosts using WSR-88D weather surveillance radar. *J. Field Ornithol.,* **69,** 316–325.

Ryzhkov, A. V., P. Zhang, R. Doviak, and C. Kessinger, 2002: Discrimination between weather and sea clutter using Doppler and dual-polarization weather radars. *Proc. 27th General Assembly of the International Union of Radio Science,* Maastricht, Netherlands, International Union of Radio Science, F1. P.3. [Available online at http://www.ursi.org/Proceedings/ProcGA02/papers/p1383.pdf.]

——, T. J. Schuur, D. W. Burgess, and D. S. Zrnić, 2005: Polarimetric tornado detection. *J. Appl. Meteor.,* **44,** 557–570.

Shusse, Y., M. Satake, S. Satoh, N. Takahashi, H. Hanado, K. Nakagawa, and T. Iguchi, 2009: Polarimetric radar observations of the eyewall of Typhoon Man-yi. Preprints, *34th Conf. on Radar Meteorology,* Williamsburg, VA, Amer. Meteor. Assoc., P13.23. [Available online at https://ams.confex.com/ams/34Radar/techprogram/paper_155998.htm.]

Southern, J., 2011: Briefs for the files. *Chat,* **76,** 19–38.

Straka, J. M., D. S. Zrnić, and A. V. Ryzhkov, 2000: Bulk hydrometeor classification and quantification using polarimetric radar data: Synthesis of relations. *J. Appl. Meteor.,* **39,** 1341–1372.

Tannehill, I. R., 1936: Tropical disturbances, June 1936. *Mon. Wea. Rev.,* **64,** 204–205.

——, 1938: Tropical disturbances of August 1938. *Mon. Wea. Rev.,* **66,** 240–241.

Thurber, W., 1980: Hurricane Fifi and the 1974 autumn migration in El Salvador. *Condor,* **82,** 212–218.

Tuck, L., 1968: Laughing gulls (*Larus atricilla*) and black skimmers (*Rynchops nigra*) brought to Newfoundland by hurricane. *J. Field Ornithol.,* **39,** 200–208.

Webster, R. E., J. Morlan, and D. Roberson, 1990: First record of the sooty tern in California. *West. Birds,* **21,** 25–32.

Williams, B., 2011: Fall 2011 coastal. *Virginia Birds,* No. 8, Virginia Society of Ornithology, Williamsburg, VA, 23 pp.

Willoughby, H. E., 1998: Tropical cyclone eye thermodynamics. *Mon. Wea. Rev.,* **126,** 3053–3067.

Yandik, W., 2011: Region 8—Hudson-Mohawk. *Kingbird,* **61,** 354–356.

Young, F. A., 1921: Weather of North America and adjacent oceans. *Mon. Wea. Rev.,* **49,** 358–359.

Zrnić, D. S., and A. V. Ryzhkov, 1998: Observations of insects and birds with a polarimetric radar. *IEEE Trans. Geosci. Remote Sens.,* **36,** 661–668.